Materials and Structures (2024) 57:208
https://doi.org/10.1617/s11527-024-02491-y

ORIGINAL ARTICLE

In situ determination of cement paste porosity in parallel with corrosion study of aluminium alloy 1100 in Portland cement pastes

Xiang Li · Sébastien Caes · Thomas Pardoen · Geert De Schutter · Tom Hauffman · Bruno Kursten

Received: 30 May 2024 / Accepted: 12 October 2024

Abstract A quantitative characterization of the capillary porosity of cement pastes has been performed in the context of corrosion of aluminium alloy 1100 in contact with Portland cement pastes. The originality of the study is to combine an electrical equivalent circuit model identified based on electrochemical impedance spectroscopy (EIS) data and a two-phase model derived from the general effective media theory (GEM). The effective resistance of the cement paste entering the GEM is approximated by the resistance of connected capillary pores as provided by the EIS analysis to determine the evolving porosity of cement pastes. Mercury intrusion porosimetry data agree with the porosity results obtained from EIS**.** The porosity in the 0.36 OPC is reduced from ~ 15% to below 10% over the first 30 days and then keeps decreasing slowly, while the porosity of the 0.36 OPC + 3% $LiNO_3$ samples slightly decreases at the beginning and finally remains constant at ~ 10%. For the 0.50 OPC + 1.607% Li_2CO_3 composition, the porosity decreases from ~ 25% to ~ 15% over the first 30 days. The influence of the curing conditions is also studied to extract the impact on the porosity**.** Besides, the diffusion of corrosion products is limited to a small region near the interface and hence the corrosion process does not affect the porosity of the cement paste.

Keywords Portland cement paste · Capillary pores · Porosity · Electrochemical impedance spectroscopy · General effective media · Mercury intrusion porosimetry

Supplementary Information The online version contains supplementary material available at https://doi.org/10.1617/s11527-024-02491-y.

X. Li · S. Caes (✉) · B. Kursten
SCK CEN, Boeretang 200, B-2400 Mol, Belgium
e-mail: sebastien.caes@sckcen.be

X. Li · T. Pardoen
Institute of Mechanics, Materials and Civil Engineering (IMMC), Université Catholique de Louvain, B-1348 Louvain-La-Neuve, Belgium

T. Pardoen
WEL Research Institute, Avenue Pasteur, 6, 1300 Wavre, Belgium

G. De Schutter
Department of Structural Engineering and Building Materials, Magnel-Vandepitte Laboratory, Ghent University, Technologiepark-Zwijnaarde 60, B-9052 Ghent, Zwijnaarde, Belgium

T. Hauffman
Department of Materials and Chemistry, Research Group Electrochemical and Surface Engineering (SURF), Vrije Universiteit Brussel, Pleinlaan 2, 1050 Brussels, Belgium

1 Introduction

The corrosion behaviour of metals in cementitious materials is significantly influenced by the behaviour of the cementitious matrix. Andrade et al. [1] reported

Published online: 24 October 2024

that the internal moisture content of chloride containing concretes controls the corrosion rate of steel inside the concrete matrix. The pH of cementitious materials also directly influences the electrochemical kinetics of metallic corrosion. For instance, steels are usually passivated in cementitious materials with high pH [2], while active metals, such as aluminium, have a high corrosion rate [3] in a highly alkaline cementitious environment. Caes et al. [4] also found that the corrosion rate of aluminium increases in cement pastes involving larger porosity.

Indeed, hardened cement paste contains a large number of pores, which play an important role in the mechanical and transport properties. Changes of the pore structure significantly influence the mechanical properties such as hardness [5], Young's modulus [6] and compressive strength [7]. Literature also shows that transport properties, including diffusion [6, 8] and permeation [9], are related to porosity, pore size, connectivity, and tortuosity of cement pastes. Because of the significant impacts on the properties, pores are usually an important factor for understanding metallic corrosion in cement pastes.

According to the size of the pores, a classification is made into two categories: gel pores smaller than 10 nm and capillary pores with size between 10 nm and 10 μm [10]. The gel pores are inner pores within the structure of hydration products such as C-S-H, CH, AF_t (Al_2O_3-Fe_2O_3-tri) and AF_m (Al_2O_3-Fe_2O_3-mono). These pores are normally regarded as part of the hydration products [11]. Capillary pores are the remnant of water-filled space initially present [12], whose volume fraction decreases with increase of hydration degree [13]. In this study, only capillary pores are considered because of their dominant role in transport mechanisms at micro-scale [14].

Electrochemical impedance spectroscopy (EIS) is a high performance technique to monitor microstructure evolution in cement pastes [15]. The frequency region above 1 kHz of the impedance spectrum of cement pastes correlates to a series of material properties such as the conductivity [16], compressive strength [17] and dielectric constant [18]. These properties are all linked to the volume fraction, size, shape and distribution of the pores in cement pastes. A series of electrical equivalent circuit models were proposed in the literature [19] based on the physical microstructure to quantitatively analyse the impedance spectrum of cement-based materials. Besides, because EIS measurements do not need to move the cement paste from the curing environment, it is considered to be an in situ technique.

In terms of electrical conductivity, the cement paste system can be roughly considered as a two-phase system with one solid-gel phase and one capillary pore phase [20–22]. Hydration products of the cement paste include C-S-H gel, CH, and other minor phases. The gel pores in the C-S-H gel are filled with physically adsorbed water, which could provide a certain level of conductivity. Other hydration products and unhydrated cement grains are normally regarded as insulators. Thus, the solid-gel phase is regarded as the low-conductivity phase. The pore solution inside the capillary pore phase contains ionic species such as OH^-,K^+, Na^+, Ca^{2+} and SO_4^{2-} [23], which dominate the charge transport process [24]. Normally, the conductivity of the solid-gel phase is much lower than the one of the capillary pore phase. Hence, the capillary pore phase is considered as the high-conductivity phase.

For a randomly distributed two-phase composite such as a cement paste, the General Effective Media (GEM) theory provides a theoretical basis to establish a physical correlation between porosity and electrical conductivity [25]. Thus, the electrical conductivity must be first experimentally measured to determine the porosity of cement-based materials through GEM approach [21, 22]. This determination usually uses AC impedance spectroscopy with a contact between cement-based materials and electrodes.

In a previous study [26], the inhibition ability of $LiNO_3$ and Li_2CO_3 on the corrosion of aluminium alloy 1100 in direct contact with Portland cement pastes was investigated using EIS, amongst other techniques. However, in addition to the information about the metal corrosion, the equivalent circuit, used to fit the EIS data, allows to gain information about the cement paste matrix, such as the resistance of connected capillary pores, without using any destructive method. Therefore, in this study, we propose the novel idea to estimate the electrical conductivity of the cement paste from the resistance of connected capillary pores. Consequently, the capillary porosity of Portland cement pastes can be quantitatively determined in parallel to the aluminium corrosion by linking the resistance of connected capillary pores (an equivalent circuit parameter) determined from

Table 1 Chemical composition of the cement

Composition	SO_3	Cl	Na_2Eq	SiO_2	Al_2O_3	Fe_2O_3	CaO	Na_2O	K_2O	MgO	Others
wt.%	2.60	0.04	0.66	21.3	5.2	3.3	63.1	0.33	0.50	2.19	0.78

Table 2 Types of cement pastes

	water/cement ratio	addition
OPC	0.36	
OPC + $LiNO_3$	0.36	3 wt.%
OPC + Li_2CO_3	0.50	1.607 wt.%

EIS fitting with the GEM theory. The influence of the corrosion on the cement paste porosity can therefore also be studied. Mercury intrusion porosimetry (MIP) measurements are then performed to examine the reliability of the porosity results obtained from this methodology.

2 Experimental procedures

2.1 Materials and sample preparation

The aluminium alloy 1100 used in the research has a chemical composition of a minimum of 99.0% Al and 1.0% Si + Fe. Specimens were cut into two different dimensions: larger Al plates (30 × 30 × 1 mm³) were used for EIS measurements, while smaller Al plates (15 × 15 × 1 mm³) were used in MIP specimens. A two-electrode configuration was adopted to measure the cement paste between two plates for EIS measurements, while the smaller aluminium plate was placed in the centre of MIP specimens. The specimens for the electrochemical measurements and MIP characterisation were prepared with Portland cement as described in the previous corrosion study [26]. In terms of the collection of cement paste pore solution, a series of pure cement paste samples was processed out of the same 40×40×40 mm^3 cubic geometry. Note that all these manipulations were performed in an Ar atmosphere glove box to create an anaerobic system. The chemical composition of Portland cement (CEM I 52,5 N class according to EN 197–1) is provided in Table 1. In this research, three different Portland cement pastes were investigated as listed in Table 2.

Figure 1 provides schematics of the three different setups used in this study. The first one (EIS setup) is used for the EIS measurements of the studied system. The MIP setup is used to collect cement paste specimens for porosity analysis by MIP (the aluminium plate inside was used for the SEM observation in the previous corrosion study [26]). Finally, the pore solution setup was produced to extract pore solution to gain information about the pore solution conductivity (see Section 4.3).

Two curing conditions were used for the cement pastes (as also previously reported in the corrosion study [26] and addressed in Section 1 of the supplementary material). The samples in condition 1 were cured in a humid Ar environment until being transferred into saturated $Ca(OH)_2$ solution after ~ 80 days (i.e. when the corrosion of Al slows down and reaches a steady state [26]). The samples in condition 2 were immersed in a saturated $Ca(OH)_2$ solution during the

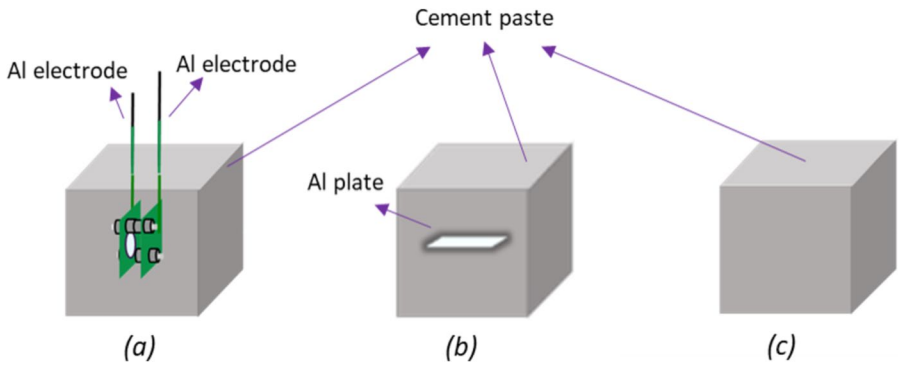

Fig. 1 Schematics of EIS **a**, MIP **b** and pore solution **c** specimens

whole experiment period. For electrochemical measurements, three repetitive samples per condition were used in order to guarantee the result repeatability. For MIP measurements, one sample was prepared at each selected time point to study the porosity variation with time. For pore solution collection, three samples were produced for each time point in order to collect enough amount of solution for the conductivity and pH measurements.

2.2 Characterisation methods

EIS measurements were done over a frequency range from 1 MHz to 10 mHz at the open circuit potential with a 10 mV amplitude of the sinusoidal potential signal. The quality of the EIS data was first examined experimentally by running the measurement first in the descending frequency step direction, i.e. from high (1 MHz) to low (10 mHz) frequencies, followed by the measurement in the ascending direction, i.e. from low to high frequencies, to confirm the stability constraint of the system. Besides, the data quality was also theoretically validated by using the Kramers–Kronig (K-K) transforms to check the linearity, causality and stability of the system. 'Zview' software was used for analysing and fitting the spectra.

MIP experiments were executed using a PASCAL 140/440 porosimeter in which the mercury pressure is linearly increased up to a maximum pressure of 200 MPa. To prepare dry samples with little microstructural damage for MIP tests, the cubic elements were immediately immersed in diethyl ether for 24 h at each selected time point. Then, the used ether solution was replaced and the sample was immersed in fresh ether for another 24 h. Finally, the sample was moved into a vacuum chamber for 24 h to evaporate the ether out of the sample. This immersion procedure into ether is applied in order to remove the water inside the cement paste and hence to stop the corrosion process and cement hydration. Afterwards, samples were cut into pieces with irregular shapes of approximately 1.5 g, taken from a corner of a specimen.

Because the conductivity of the cement pore solution needs to be known for the application of the GEM theory, the cement pore solution was experimentally collected from the cement paste samples. A universal testing machine with corresponding accessories (a plunger, a hollow steel tube and a pedestal) was used to extract solution from the samples (Part 2 in the supplementary material). The paste sample was placed in the hollow tube, then the testing machine imposed a compressive force up to 900 kN on the plunger. The pore solution squeezed out from the paste sample was collected in a ring-like reservoir in the pedestal. A series of cement samples were produced and squeezed to collect cement pore solutions during 120 days, followed by conductivity and pH measurements (see Section 4.3).

3 General effective media

A methodology is proposed to determine the cement paste porosity based on EIS results. The first step is the construction of an appropriate model to relate the electrical resistivity and the cement paste porosity. Because of the complexity of cement paste as a compound system, the model has to be simplified compared to reality by retaining only the dominant micro structural parameters, e.g. porosity and tortuosity.

General Effective Media (GEM) model, proposed by McLachlan et al. [25], combines percolation and EMT theories and puts forward a mathematical equation linking the electrical conductivity (=1/resistivity) values with the microstructure parameters, given by [25]:

$$\phi = \frac{\left[\left(\frac{\sigma_p}{\sigma_{eff}}\right)^{\frac{1}{t}} + \left(\frac{1-\phi_c}{\phi_c}\right)\right]\left[\left(\frac{\sigma_s}{\sigma_{eff}}\right)^{\frac{1}{t}} - 1\right]}{\left[\left(\frac{\sigma_p}{\sigma_{eff}}\right)^{\frac{1}{t}} + \left(\frac{1-\phi_c}{\phi_c}\right)\right]\left[\left(\frac{\sigma_s}{\sigma_{eff}}\right)^{\frac{1}{t}} - 1\right] - \left[\left(\frac{\sigma_p}{\sigma_{eff}}\right)^{\frac{1}{t}} - 1\right]\left[\left(\frac{\sigma_s}{\sigma_{eff}}\right)^{\frac{1}{t}} + \left(\frac{1-\phi_c}{\phi_c}\right)\right]} \quad (1)$$

where ϕ is the volume fraction of the low-resistivity phase, i.e. porosity, ϕ_c is the percolation threshold of the capillary pores, t is the critical exponent revealing

the conductivity of the conducting regions in the microstructures, σ_p is the conductivity of the capillary pore phase, and σ_s is the conductivity of the solid-gel phase. These different parameters are discussed one by one hereafter to explain how the identification is performed based on literature data or on experimental results.

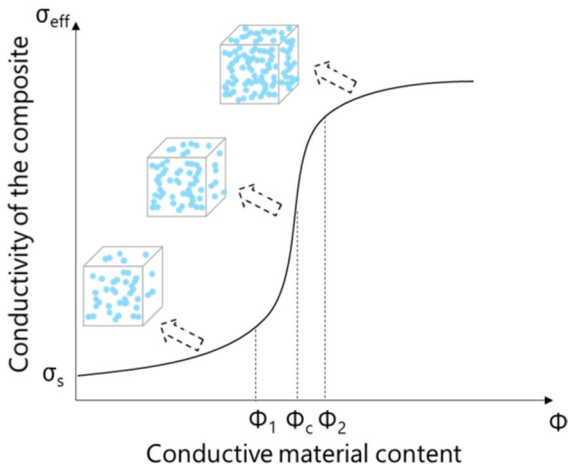

Fig. 2 Relationship between the effective conductivity and porosity in cement pastes

3.1 Percolation threshold ϕ_c of the capillary pores

The percolation threshold of the cementitious material is the point at which the system is firstly interconnected by the capillary pores, i.e., the first appearance of long-range connectivity. It can be seen in Fig. 2 that the effective conductivity of the cement paste increases significantly at around ϕ_c due to the connection of individual pores. According to literature [13, 27, 28, 32], ϕ_c is independent of the water/cement ratio. Garboczi et al. [29] studied the percolation of the cement paste by modeling their studied system with a three-dimensional digital image. When a high resolution of 400^3-pixels (0.25 µm/pixel) is chosen, the threshold is 0.12, which corresponds with the result obtained in the multi-scale model of Prabhu et al. [30]. Besides, ϕ_c decreases in this model with the increment of the digital resolution, meaning that the smaller the pores taken into account, the smaller the ϕ_c. Navi et al. [31] also found a similar relationship between the percolation threshold and the resolution in their mathematical model. They reported that in normal cement pastes, with a 10% total porosity, more than 95% of capillary pores are connected under a 2 µm/pixel resolution. Tumidajski et al. [32] experimentally tested the porosity and the electrical

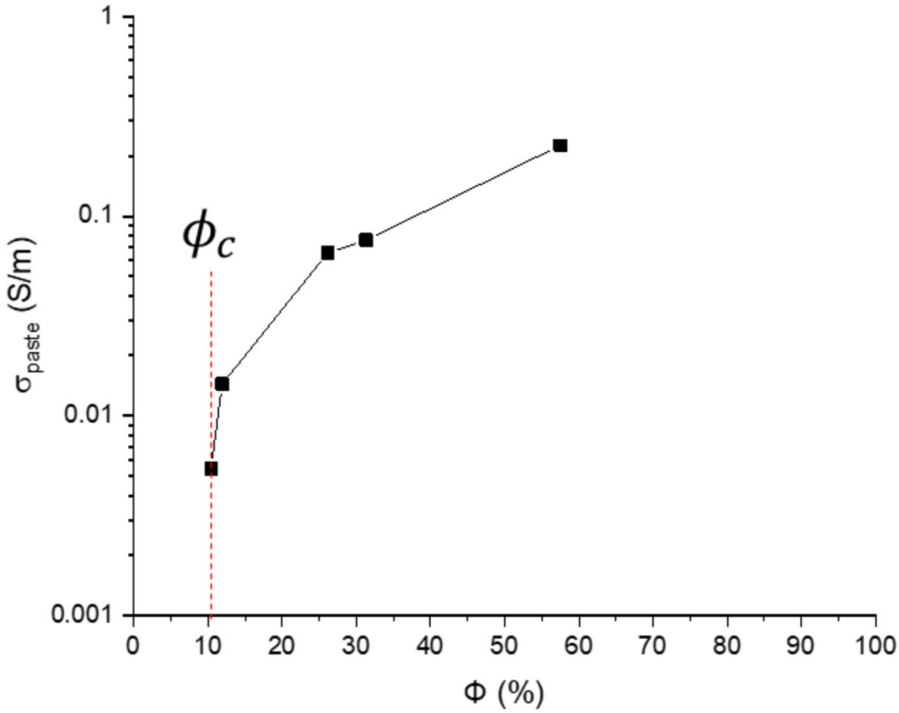

Fig. 3 Variation of the conductivity of cement pastes as a function of porosity as determined by Tumidajski et al. [32]

resistivity of different cement pastes. Figure 3, drawn according to their results, shows that the conductivity (1/resistivity) changes most significantly at around 10.4%, which fulfils the definition of the percolation threshhold. Hence, $\phi_c = 0.104$ was selected in the present study.

3.2 Critical exponent t

The larger the t value, the more tortuous the network, or the rougher the surface of the conductor. Different ranges of t are reported in literature. Theoretical lattice models are used to predict t in an ideal 3D lattice system providing a t value equal to 2 [33]. McLachlan et al. [25] and Isichenko [34] reported that t ranges between 1.4 and 2.46 for composites based on computation simulations. Other researchers adopted $t=2$ [21, 28]. In the present study, we retain the value $t=2$ for all cement pastes because it is most widely used for the cementitious materials.

3.3 Conductivity of capillary pore phase σ_p

When the cement paste is fully saturated, the capillary pores are entirely filled with pore solution and σ_p is equal to the conductivity of the pore solution. When the capillary pores are partly saturated, σ_p is lower than the conductivity of the pore solution until reaching zero when the capillary pores are dry. The different saturation conditions are illustrated in Fig. 4. The pore solution conductivity can be obtained directly by extracting and measuring the pore solution from the cementitious materials. Buenfeld et al. [35] reported that the pore solution resistivity is in the range of 0.3–0.4 Ω·m (i.e. 2.5–3.3 S/m for the σ_p conductivity), with a small change over 4–20 weeks for OPC mortar of 0.4 and 0.6 water/cement ratios. In this study, the conductivity of the pore solutions was experimentally measured as addressed in Section 4.3 and was used for the value of σ_p. Note that the use of the conductivity of the pore solution for σ_p leads to an underestimation of the calculated porosity when the pores are not fully saturated. It is as if only the space occupied by the pore solution is taken into account, while the empty pore space is regarded as part of the solid-gel phase.

3.4 Conductivity of solid-gel phase σ_s

The conductivity σ_s for OPC pastes is difficult to be directly measured. Zhang et al. [21] proposed that the appropriate value of σ_s/σ_p ranges from 10^{-3} to 10^{-2} and chose a value of 0.0025 in their model. Neithalath et al. [22] used $\sigma_s = 0.0075$ S/m, which is close to the value in the study of Ma et al. [36]. Christensen et al. [37] reported that σ_s is estimated as equal to $(1-\phi)\times 10^{-3}$ S/m. The work of Garboczi et al. [28] estimated that σ_s/σ_p varies continuously between 0.001 and 0.0025. Oh et al. [27] deduced the value of σ_s/σ_p according to the relationship between the effective diffusivity and the conductivity. They reported that the value of σ_s/σ_p is about 2.0×10^{-4} for OPC pastes. In this study, σ_p will be shown to be in the range from 7 to 16 S/m (see Section 4.3) and hence σ_s should range from 0.00035 to 0.0008 S/m. In fact, it is very likely that σ_s slightly fluctuates. On the one hand, many factors e.g. the setting time, the composition and the curing condition, can play a role, which lead to different σ_s values. On the other hand, the main contribution for the solid-gel phase conductivity should always come from the C-S-H phase in all types of OPC

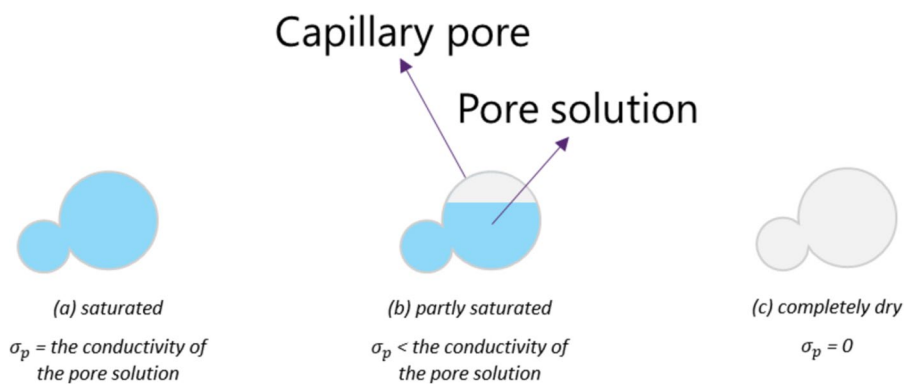

Fig. 4 The different saturation conditions of capillary pores

pastes, which means that the σ_s range is limited. In this study, 0.0008 S/m has been selected as a fixed σ_s value. In fact, σ_s and σ_p have a relatively low influence on the porosity compared with ϕ_c, t and σ_{eff}. Trials on different values indicate that there is just an insignificant effect on the porosity result no matter 0.001 S/m, 0.0008 S/m or even 0.00035 S/m is chosen.

3.5 Conductivity of overall cement paste σ_{eff}

The effective conductivity σ_{eff} is regarded as a homogenized material property. The relationship between the resistance and the conductivity is given by Eq. (2):

$$\sigma_{\text{eff}} = \frac{K}{R_{\text{eff}}} \tag{2}$$

where K is the cell constant and R_{eff} is the effective resistance of the system. The value of K is only determined by the geometry of the electrochemical cell and is fixed for a specific cell, irrespective of the type of electrolyte. Hence, in order to determine the K value, an impedance experiment was carried out in saturated $Ca(OH)_2$ solution using the same two-electrode cells as the ones cast in the cement pastes. EIS tests were then carried out in a frequency range of 1 MHz to 10 mHz using a 10 mV peak-to-peak AC potential signal. The impedance of the system in the very high frequency domain fluctuates at around 100 Ω and could be regarded as the R_{eff} of the cell in saturated $Ca(OH)_2$ solution (see Part 3 in the supplementary material). The conductivity σ_{eff} of the saturated $Ca(OH)_2$ test solution was experimentally measured by a conductivity meter and was found to be 1.03 S/m. Therefore, the K value was calculated to be equal to 103 as determined by Eq. (2). Using R_{eff} in saturated $Ca(OH)_2$ solution and σ_{eff} of saturated $Ca(OH)_2$ solution. Then R_{eff} of the cement paste is still needed to calculate σ_{eff} of the cement paste. R_{eff} changes as a function of the pore content as shown in Fig. 2 and will be provided by the fitting of the equivalent circuit in Section 4.2.

4 Results and discussion

4.1 Impedance spectra

Three frequency domains can be distinguished in the impedance spectra of pure OPC samples shown in Fig. 5. The first semicircle in the high frequency domain is related to the cement paste, while the arc at the low-frequency limit reveals the response of the interface between the aluminium and cement paste,

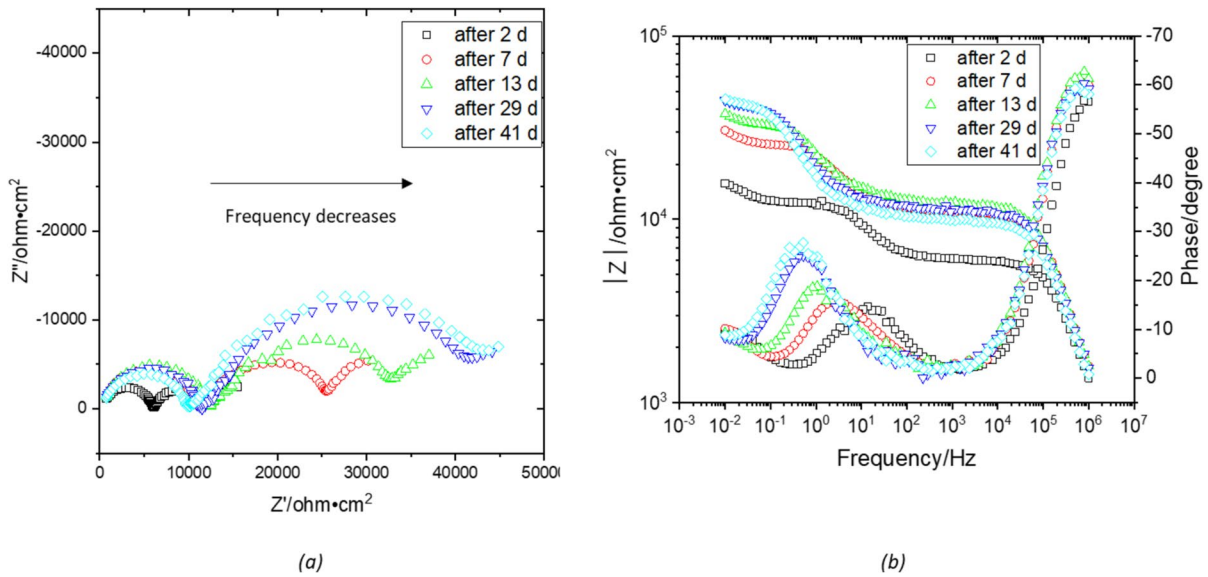

Fig. 5 Variation of Nyquist **a** and Bode plots **b** of AA1100 with time in pure OPC paste under condition 1

including a corrosion product film. Another semicircle is observed in the medium frequency region accounting for the impedance responses provided by both the cement paste and the interface. The three domains are also found when measuring samples with the addition of $LiNO_3$ or Li_2CO_3: (i) in the high-frequency domain, (ii) around the 1 ~ 10 Hz domain and (iii) in the low-frequency domain, respectively. Exceptionally, a fourth domain in the 1 ~ 10 kHz range is observed in an OPC + Li_2CO_3 sample. Similar explanations can be found in the literature regarding the impedance plots in cementitous systems [16], but a direct comparison might bring errors because of the influential differences associated to the cement paste composition, to the experimental set-up and to the curing enviroment.

An example of the Nyquist impedance spectra of the pure OPC sample in conditon 1 is provided in Fig. 5. The sample changes as a function of time with the following phenomena: (i) the water content of the cement paste decreases with ongoing cement hydration, (ii) the thickness of the corrosion product film monotonically increases and the corrosion rate of Al reduces fast at the beginning. Some information are directly revealed in the impedance spectra. For example, all these physical variations mentioned above lead to the resistance increase of the sample. Correspondingly, in the Bode plots as shown in Fig. 5b, the absolute value of the impedance increases monotonically as a function of time, especially during the first 28 days of the test. Afterwards, the impedance increases with a lower rate. The arc in the low-frequency domain, which corresponds to the interfacial response, gradually overlaps with the intermediate semicircle. This is attributed to the overlapping of the time constants, which are situated in the same frequency region. In terms of the impedance plots of other samples, the same problem of overlapping time constants brings difficulties to analyse impedance results only by visual observation of the Nyquist and Bode plots. Hence, the fitting of the impedance spectrum was needed to quantitatively obtain more useful information.

4.2 Equivalent circuit model

The EIS spectrum was fitted using the electrical equivalent circuit (EEC) presented in Fig. 6, which has been previously utilised in a corrosion study [26], for the quantitative analysis of the spectrum results.

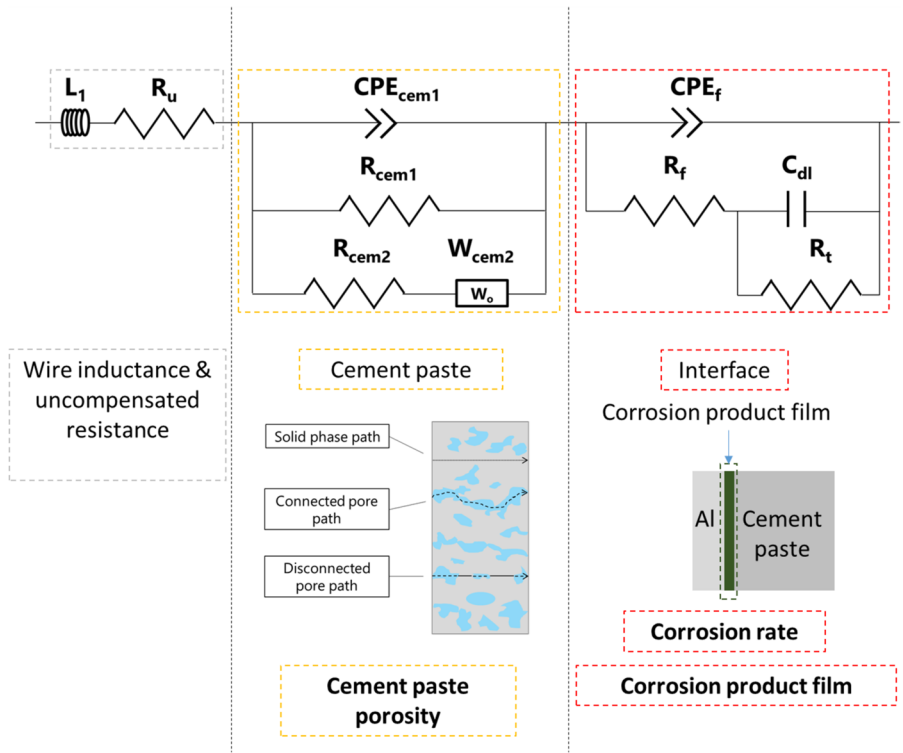

Fig. 6 Electrical equivalent circuit used to fit the EIS spectra for the corrosion of Al plate in cement pastes

The EEC was constructed based on the physical structure of the cell and consists of three different parts.

The first part consists of an inductor (L_1) and a resistor (R_u) placed in series. L_1 represents the inductance of the external wires. R_u is the overall uncompensated resistance including the resistance of the aluminium plate, Al rods, the connecting cables and the pore solution in the crevices or macro holes of the cementitious matrix. L_1 and R_u are used or not depending on the quality of the fitting result. Please note that this selection has negligible impact on the other parts of the circuit.

The second section of the circuit is composed of three parallel branches, which describe the electrochemical responses of the cement paste between both working and counter electrodes. CPE_{cem1} corresponds to the capacitance properties of the solid phase of the cement paste; R_{cem1} represents the resistance related to the ionic conduction provided by the connected capillary pores; the branch composed of a resistor (R_{cem2}) and a Warburg element (W_{cem2}) describes the charge transport processes inside the disconnected capillary pores and the solid phase between these disconnected pores. The construction of this model was based on the work of Marriaga et al. [38] and discussed in the previous research [26] (see also Part 4 of the supplementary material). Considering the significant conductivity difference between the solid-gel phase and the pore solution (see Section 3.4), the contribution of the solid phase path and of the disconnected pore path could be negligible when determining the effective resistance of the cement paste under a direct current state. In other words, the effective resistance of the cement paste mainly depends on the resistance of the connected capillary pores. Consequently, the effective resistance of the cement paste, R_{eff} (its definition is provided in Section 3.5), can be approximated by R_{cem1}.

The third part of the EEC has been used to study the corrosion of aluminium alloy 1100 in contact with Portland cement pastes [26]. It describes the electrochemical responses of the cement paste / corrosion product film / aluminium interface. R_f and CPE_f (C_f if the 'n' value of CPE_f is equal to 1 in the fit) account for the resistance and the capacitance properties of the corrosion product film, respectively. C_{dl} represents the double layer capacitance. R_t is the charge transfer resistance, which reveals the difficulty encountered when an electron is shifted on the interface.

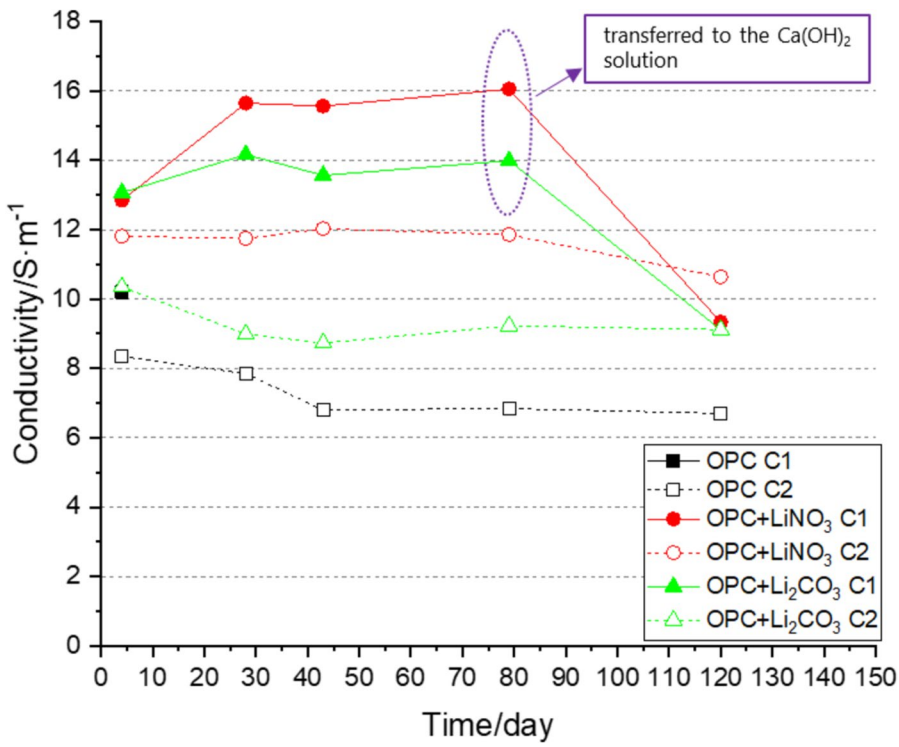

Fig. 7 Variation of the conductivity of cement pore solution as a function time for different conditions with or without inhibitors

4.3 The conductivity and pH of pore solution

Once the cement pore solution was collected by the squeezing method, the conductivity and pH values were measured by conductivity and pH meters, respectively. The results of the conductivity measurements of the squeezed cement pore solutions are given in Fig. 7. One solution sample was collected for each type of cement paste at each time point. Generally, the pore solution conductivity of each cement paste is almost constant in a specific curing condition. Note that the data for the 0.36 w/c OPC cement paste specimens, tested in condition 1 and without the addition of lithium salts, are missing after 4 days because no pore solution could be collected out of the specimens. This is due to the fact that the low water/cement ratio equal to 0.36 is the minimum ratio for full hydration of cement grains, causing the lack of residual water inside the cement paste [39, 40]. However, no problem occurred for OPC + $LiNO_3$ samples with the same w/c ratio. Some studies [41] reported that the Li ions can be incorporated into the C-S-H at the early stages of the hydration through the occupation of calcium sites in the C–S–H-like structure. This absorption may contribute to a decrease of the interlayer water or of the physically adsorbed water in C-S-H and hence can rise the water level in capillary pores. Further researches are needed to confirm this hypothesis. The conductivity values of pore solution for all samples in condition 2 remain relatively constant over time. For samples cured in condition 1, the conductivity values are almost stable (a small increase can be seen at the beginning) until they significantly decrease towards values close to those measured for samples cured in condition 2 after the immersion of samples in saturated $Ca(OH)_2$ solution. Besides, it can be clearly seen that the addition of lithium salts increases the conductivity. The conductivity decreases in the following order: [OPC + $LiNO_3$] > [OPC + Li_2CO_3] > OPC. This trend is found for both conditions. Furthermore, the conductivity in condition 2 is lower than that in condition 1. This is caused by the higher availability of water in condition 2 (compared to condition 1) resulting in a stronger dilution of the ion concentrations and consequently in a reduction of the conductivity. Indeed, the specimens in condition 2 are immersed in the saturated $Ca(OH)_2$ solution. Therefore, $Ca(OH)_2$ solution can go through the connected pores and dilute the pore solution, decreasing the conductivity of the pore solution. This was also reported that the curing environments can change the chemistry of the pore solution [42, 43]. The conductivity value for each cement paste in a specific curing condition is regarded as a constant with ongoing cement hydration (see Table S1 in Section 5 of the supplementary material) and is used for the value of σ_p in the GEM model. This matches the results in literature addressed in Sect. 3.3, in which the conductivity value of cementitious materials is stable with ongoing cement hydration.

Figure 8 illustrates the variation of pH of the pore solution with time. The enhanced pH reported by Diamond [44] when adding Li_2CO_3 is not observed in our results. By contrast, the addition of $LiNO_3$ and Li_2CO_3 seems to decrease the pH in comparison to pure OPC systems without any lithium addition. In general, all samples showed a high pH, above 12.

4.4 Comparison of porosity results

After having determined all the parameters of the GEM model (see Sect. 3 and Sect. 4.3), the porosity was estimated using Eq. (1). The porosity evolution of three types of cement pastes (Portland cement pastes of a 0.36 water/cement ratio with/without the addition of 3 wt.% $LiNO_3$ and Portland cement paste of a 0.50 water/cement ratio with 1.607 wt.% Li_2CO_3) in two kinds of curing conditions (in humid Ar and in saturated $Ca(OH)_2$ solution) was studied. These three different pastes and two conditions were studied to examine the reliability of the proposed methodology.

A comparison of the porosity determined by EIS and MIP is shown in Fig. 9. For the 0.36 OPC specimens in condition 1 (Fig. 9a), the tests are stopped after 40 days because scatter in impedance plots increases as a function of time [26], consequently leading to the difficulties of obtaining reliable fitting results and the failure of porosity determination after 40 days. This should be attributed to the accumulation of corrosion products and the generation of H_2 caused by the fast corrosion of Al, leading to cracks and holes inside the corrosion product film and the cement paste. These cracks and holes were found by SEM already after 28 days (Fig. 10) and also at the surface of the cement paste blocks after 133 days (see Figure S9a in Sect. 6 of the supplementary material).

The porosity extracted from EIS decreases from about 15% to around 8% over the first 15 days and

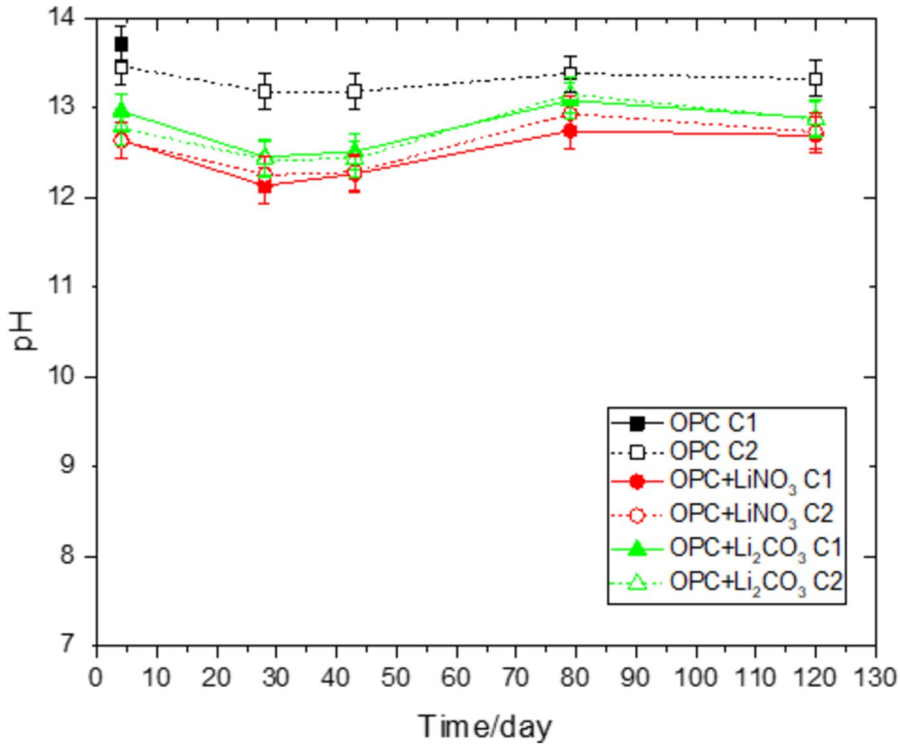

Fig. 8 Variation of the pH of cement paste pore solutions as a function of time

remains constant afterwards. The porosity extracted from the MIP measurements also declines during the first 30 days, then remains constant and finally decreases after 80 days. This second decrease is likely linked to the transfer of the cement paste specimen into saturated $Ca(OH)_2$ solution after 80 days of testing with the precipitation of $Ca(OH)_2$ probably occluding the connected pores. From Fig. 9a, it is also apparent that the porosity values obtained from EIS are slightly lower than the values measured with MIP. This is caused by the characteristics of the EIS method, i.e. either the occlusion of pores by corrosion products or the unsaturation of pores because of pore solution deficiency. First, the corrosion products probably occlude the cement pores thereby decreasing the porosity measured by EIS. Indeed, the distribution of the aluminium (Fig. 10), which mainly comes from the corrosion products, indicates that the corrosion products have the tendency of diffusing towards the cement paste matrix as the Al content decreases with increasing distance from the interface. This occlusion could be especially severe when there is no protection of a dense corrosion product film in these 0.36 OPC samples (the corrosion products were rapidly generated without the addition of lithium). However, the influence of the diffusion is limited in a small district within a few tens of micrometres away from the interface between the corrosion product film and the cement paste, even if the corrosion in 0.36 OPC samples is fast. Moreover, the corrosion products can also incorporated into the solid phase of the cement paste instead of directly occluding the pores. For instance, the C-S-H gel is capable of partially substituting Si by Al, forming C-A-S-H [45]. Therefore, the diffusion of the corrosion products does not seem to significantly impact the measurement of the cement paste porosity. Another explanation is that the porosity measured by EIS is related to the amount of cement paste pore solution. In this research, the conductivity of the pore solution was measured and was used as the conductivity of capillary pore phase σ_p in the GEM theory, which is only appropriate when the capillary pores are entirely filled with pore solution as shown in Fig. 4a. When the capillary pores are only partly filled with pore solution (Fig. 4b), this approximation leads to an underestimation of the porosity. The amount of pore solution is determined by numerous factors, such as humidity and initial water/cement ratio. In the hydration process, the rapid consumption of the pore solution results in a lack of pore solution

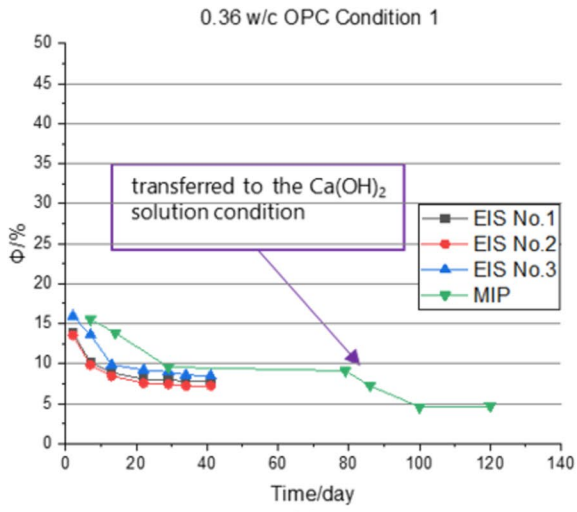
0.36 w/c OPC Condition 1
transferred to the Ca(OH)2 solution condition
EIS No.1
EIS No.2
EIS No.3
MIP
Φ/%
Time/day

(a)

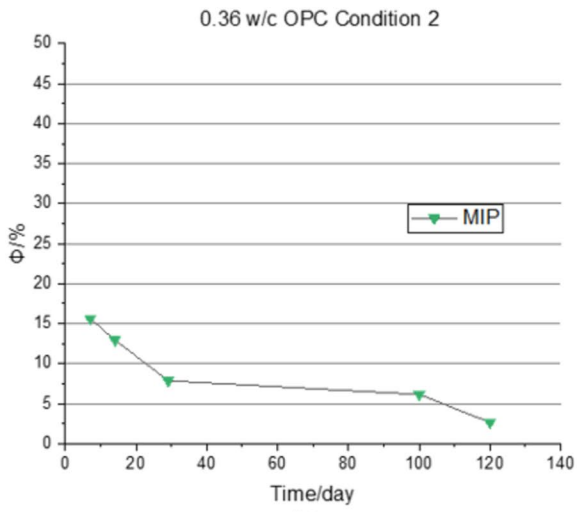
0.36 w/c OPC Condition 2
MIP
Φ/%
Time/day

(b)

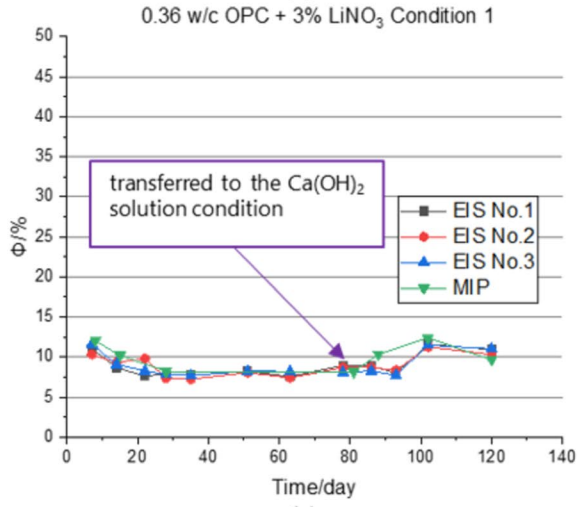
0.36 w/c OPC + 3% LiNO3 Condition 1
transferred to the Ca(OH)2 solution condition
EIS No.1
EIS No.2
EIS No.3
MIP
Φ/%
Time/day

(c)

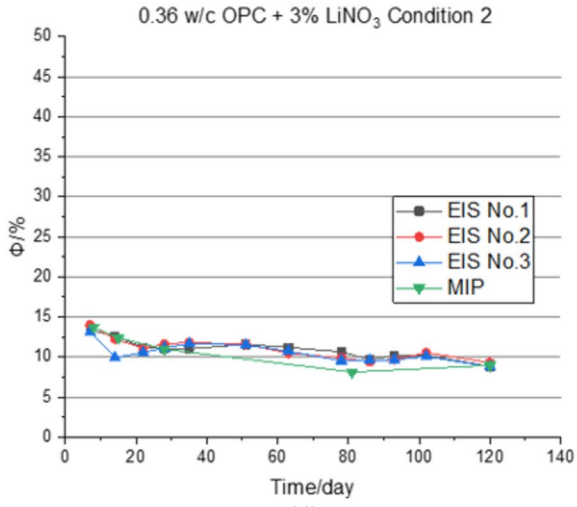
0.36 w/c OPC + 3% LiNO3 Condition 2
EIS No.1
EIS No.2
EIS No.3
MIP
Φ/%
Time/day

(d)

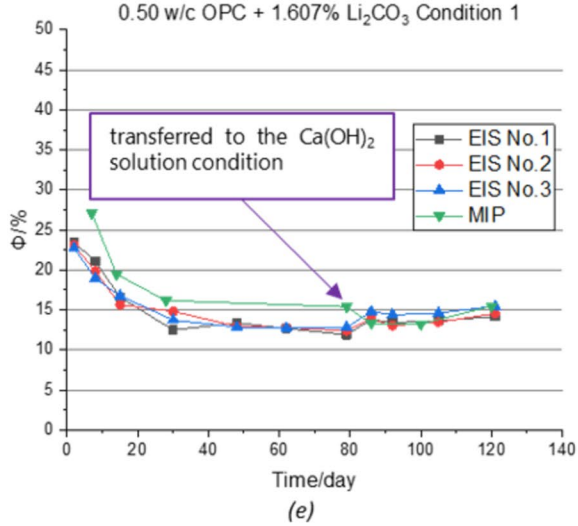
0.50 w/c OPC + 1.607% Li2CO3 Condition 1
transferred to the Ca(OH)2 solution condition
EIS No.1
EIS No.2
EIS No.3
MIP
Φ/%
Time/day

(e)

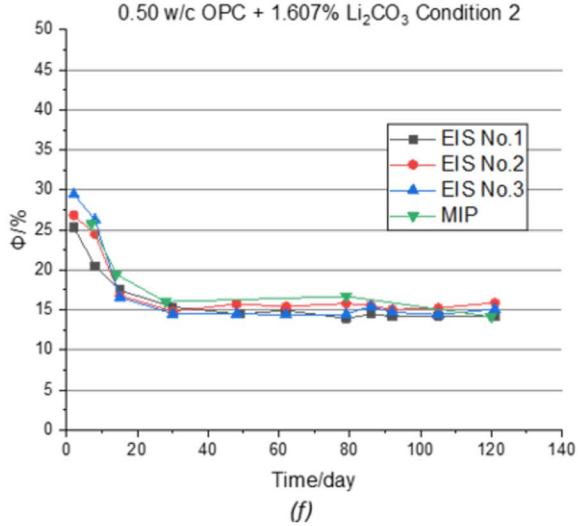
0.50 w/c OPC + 1.607% Li2CO3 Condition 2
EIS No.1
EIS No.2
EIS No.3
MIP
Φ/%
Time/day

(f)

◂**Fig. 9** Variation of the porosity as a function of time measured by EIS and MIP of **a** 0.36 OPC samples in condition 1, **b** 0.36 OPC samples in condition 2, **c** 0.36 OPC + 3% $LiNO_3$ samples in condition 1, **d** 0.36 OPC + 3% $LiNO_3$ samples in condition 2, **e** 0.50 OPC + 1.607% Li_2CO_3 samples in condition 1, **f** 0.50 OPC + 1.607% Li_2CO_3 samples in condition 2

for filling in all capillary pores. Besides, the extra water consumption caused by the corrosion process probably intensifies this solution deficiency. Hence, this pore solution deficiency could be the reason for the porosity from EIS to be lower than that from MIP.

In condition 2 (Fig. 9b), only the porosity results from MIP are shown because it was not possible to obtain valuable information from the EIS measurements since all samples breached soon after the start of the tests (Figure S9b in Sect. 6 of the supplementary material). Cui et al. [20] reported that the porostiy values for OPC pastes of 0.3 and 0.4 water/cement ratios are 5.9% and 9.1% respectively after a long hydration period (210 days), which is similar to the results obtained by MIP in this study.

Figure 9c and d provide the porosity results of 0.36 OPC + 3% $LiNO_3$ samples obtained from EIS and MIP measurements. The minor difference observed between the porosities measured with EIS and MIP probably means that 0.36 OPC + 3% $LiNO_3$ samples contain enough pore solution to fill all the capillary pores even in a humid Ar atmosphere at the beginning of the tests done in condition 1. This is consistent with the fact that more pore solution could be extracted from the 0.36 OPC + 3% $LiNO_3$ samples compared to the 0.36 OPC samples. As addressed in Section 4.3, no pore solution was collected out of the 0.36 OPC samples after 4 days or later in condition 1, while enough solution was successfully collected when 3% $LiNO_3$ was added to samples with the same w/c ratio, proving the increase of the amount of pore solution caused by $LiNO_3$ addition. In condition 1, the porosity value of the 0.36 OPC + 3% $LiNO_3$ samples slightly decreases during the first 20 days and then keeps stable at around 10% until immersion of the cement paste samples in saturated $Ca(OH)_2$ solution. After the immersion, MIP shows that the porosity increases instantly, which can be attributed to the fast leaching of salts, i.e. $LiNO_3$, inside the cement paste into the solution, while it takes a longer time to observe the same increase in EIS technique. This retardation in EIS can be explained by the longer diffusion path of salts in EIS samples (MIP measures the porosity in the corner of a specimen, while EIS measures the porosity in the middle of the cement paste as explained in Sect. 2.1). In condition 2, the porosity slightly decreases to about 10% at the beginning followed by a long steady state measured until the end of the test.

A comparison of the porosity results obtained from EIS and MIP measurements for 0.50 OPC + 1.607% Li_2CO_3 are provided in Fig. 9e and f. For samples in condition 1, the porosity values measured from EIS and MIP follow the same trend until immersion of the cement paste samples in saturated $Ca(OH)_2$ solution on the 80th day. However, the absolute values obtained from EIS are clearly lower than that from MIP. Similar to the situation of 0.36 OPC samples in condition 1, this might be caused by a lack of pore solution. After 80 days, the porosity from EIS increases slightly and then remains fairly the same as those obtained from MIP. This increase is likely due to the fact that immersion of the cement paste samples in saturated $Ca(OH)_2$ solution provided enough water to fill all the pores in the cement paste, and hence higher porosity values were measured. In condition 2, the results from EIS and MIP are identical, showing that data obtained by EIS can be efficiently used for the determination of the cement porosity. In both conditions, the porosity obtained from MIP drops from above 25% after 7 days to about 15% after 28 days. Boel et al. [46] studied the porosity variation of OPC pastes and reported a porosity decrease from about 22% after 14 days to about 16% after 3 months for the cement paste of 0.50 water/cement ratio. Hence, the addition of 1.607% Li_2CO_3 has little impact on the porosity variation.

Considering the influence of the corrosion products on the cement paste, if the corrosion products would occlude a large fraction of the pores and effectively decrease the total porosity, this would lead to an enhancement of the strength of the cement paste. However, the diffusion of corrosion products is found to be limited to a narrow region near the interface and cannot thus induce significant change of total porosity. Now, the accumulation of corrosion products increases the internal stress resulting in cracking of the cement pastes. Therefore, the corrosion products from Al are detrimental to the cement pastes.

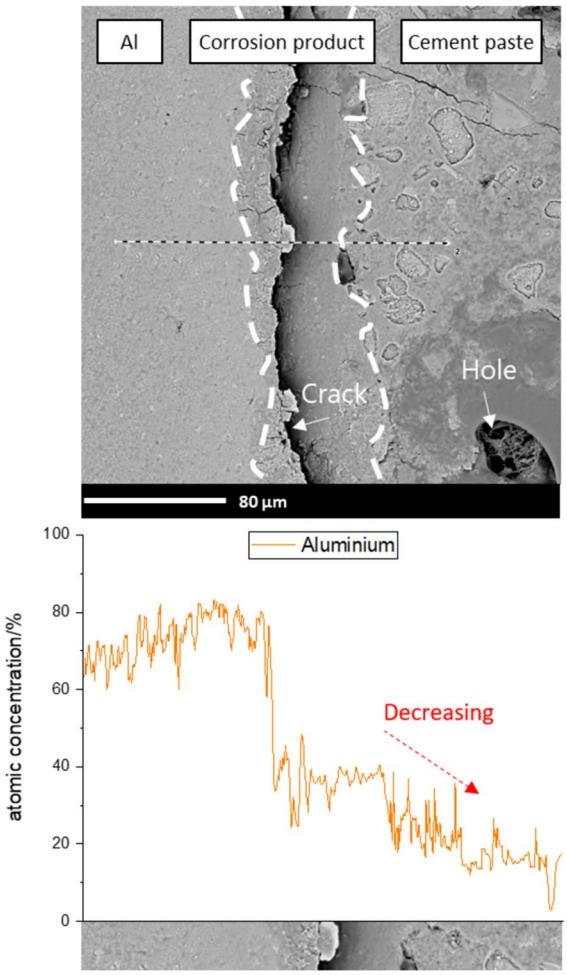

Fig. 10 SEM and EDX line scan results of the Al element of the cross-section of an OPC sample in condition 1 for 28 days

5 Conclusions

This paper describes the possibility to generate quantitative in situ information on the porosity of cement paste by combining EIS with the General Effective Media (GEM) theory. The main findings of the research are the following:

1. The pore solution conductivity of each cement paste is almost constant in a specific curing condition, which evidences that the conductivity value only needs to be measured once. Meanwhile, the pH values of the pore solutions are also measured and all samples show a high pH, above 12.
2. The porosity results obtained from EIS and MIP are in good agreement, proving the effectiveness of the methodology. The porosity of the 0.36 OPC reduces fast from ~ 15% to below 10% and then keeps slowly decreasing. The porosity of the 0.36 OPC + 3% $LiNO_3$ composition decreases slightly at the beginning and finally reaches a steady state value of ~ 10%. For the 0.50 OPC + 1.607% Li_2CO_3, the porosity significantly decreases from a high level of ~ 25% to ~ 15% over the first 30 days.
3. The corrosion products have the tendency of diffusing towards the cement paste matrix, but the diffusion is limited in a small district within a few tens of micrometres away from the interface and hence does not seem to influence the measurement of the cement paste porosity.
4. The partly saturated pores lead to an underestimation of the total porosity in this novel methodology. After more solution (i.e. the immersion of samples in saturated $Ca(OH)_2$ solution) was provided to fill all the pores in the cement paste, the porosity values measured by EIS increase to the level of MIP.
5. The addition of $LiNO_3$ probably results in an increase of the pore solution amount, providing enough water to saturate the all the pores.

Besides the context of corrosion of aluminium alloy 1100 in contact with Portland cement pastes, the present work proves, that EIS can simultaneously provide in situ porosity information. This novel methodology can be applied to other problems including for instance the carbonation of concretes, in which both the corrosion of rebars and the porosity of concrete need to be studied.

Acknowledgements The work was financially supported by the 'Technical Passive fund' of the Belgian state and was under the framework of the cooperation between ONDRAF/NIRAS and SCK CEN.

Author contributions Xiang Li: Investigation, Data Curation, Writing—Original Draft, Writing—Review and Editing, Visualization, Methodology. Sébastien Caes: Writing—Review and Editing, Visualization, Methodology, Validation, Project administration. Thomas Pardoen: Writing—Review and Editing, Methodology, Resource. Geert De Schutter: Writing—Review & Editing, Methodology. Tom Hauffman: Writing—Review and Editing, Methodology. Bruno Kursten: Writing—Review and Editing, Methodology, Validation.

Funding The authors declare the following financial interests/personal relationships which may be considered as potential competing interests.

Declarations

Conflict of interest The authors declare that they have no known competing financial interests or personal relationships that could have appeared to influence the work reported in this paper.

References

1. Andrade C, Alonso C, Sarría J (2002) Corrosion rate evolution in concrete structures exposed to the atmosphere. Cement Concr Comp 24:55–64. https://doi.org/10.1016/S0958-9465(01)00026-9
2. Poursaee A, Hansson C (2007) Reinforcing steel passivation in mortar and pore solution. Cement Concr Res 37:1127–1133. https://doi.org/10.1016/j.cemconres.2007.04.005
3. Spasova L, Ojovan M (2008) Characterisation of Al corrosion and its impact on the mechanical performance of composite cement wasteforms by the acoustic emission technique. J Nucl Mater 375:347–358. https://doi.org/10.1016/j.jnucmat.2007.11.010
4. Caes S, Gurning AC, Li X, De Souza V, Kursten B (2023) Corrosion of aluminium in ordinary Portland cement paste: influence of matrix porosity and the presence of $LiNO_3$ corrosion inhibitor. Mater Corros 74:125–137. https://doi.org/10.1002/maco.202213296
5. Liu L, Wang X, Zhou J, Chu H, Shen D, Chen H, Qin S (2018) Investigation of pore structure and mechanical property of cement paste subjected to the coupled action of freezing/thawing and calcium leaching. Cement Concr Res 109:133–146. https://doi.org/10.1016/j.cemconres.2018.04.015
6. Šavija B, Zhang H, Schlangen E (2019) Assessing hydrated cement paste properties using experimentally informed discrete models. J Mater Civil Eng 31:04019169. https://doi.org/10.1061/(ASCE)MT.1943-5533.0002772
7. Li L, Zhang H, Guo X, Zhou X, Lu L, Chen M, Cheng X (2019) Pore structure evolution and strength development of hardened cement paste with super low water-to-cement ratios. Constr Build Mater 227:117108. https://doi.org/10.1016/j.conbuildmat.2019.117108
8. Ngala V, Page C (1997) Effects of carbonation on pore structure and diffusional properties of hydrated cement pastes. Cement Concr Res 27:995–1007. https://doi.org/10.1016/S0008-8846(97)00102-6
9. Jiang ZL, Pan YJ, Lu JF, Wang YC (2022) Pore structure characterization of cement paste by different experimental methods and its influence on permeability evaluation. Cement Concr Res 159:106892. https://doi.org/10.1016/j.cemconres.2022.106892
10. Gao P, Ye G, Wei J, Yu Q (2015) Multi-scale simulation of capillary pores and gel pores in Portland cement paste. In: 14th international congress on the chemistry of cement 1–14.
11. Jennings HM (2004) Colloid model of C− S− H and implications to the problem of creep and shrinkage. Mater Struct 37:59–70. https://doi.org/10.1007/BF02481627
12. Taylor HF (1997) Cement chemistry. Thomas Telford, London
13. Ye G (2005) Percolation of capillary pores in hardening cement pastes. Cement Concr Res 35:167–176. https://doi.org/10.1016/j.cemconres.2004.07.033
14. Ma H, Li Z (2013) Realistic pore structure of Portland cement paste: experimental study and numerical simulation. Comput Concr 11:317–336. https://doi.org/10.12989/cac.2013.11.4.317
15. Gu P, Xie P, Fu Y, Beaudoin J (1994) AC impedance phenomena in hydrating cement systems: frequency dispersion angle and pore size distribution. Cement Concr Res 24:86–88
16. Díaz B, Guitián B, Nóvoa XR, Pérez C (2021) Conductivity assessment of multifunctional cement pastes by impedance spectroscopy. Corros Sci 185:109441. https://doi.org/10.1016/j.corsci.2021.109441
17. Tang S, Li Z, Shao H, Chen E (2014) Characterization of early-age hydration process of cement pastes based on impedance measurement. Constr Build Mater 68:491–500. https://doi.org/10.1016/j.conbuildmat.2014.07.009
18. Keddam M, Takenouti H, Novoa X, Andrade C, Alonso C (1997) Impedance measurements on cement paste. Cement Concr Res 27:1191–1201. https://doi.org/10.1016/S0008-8846(97)00117-8
19. Andrade C, Blanco V, Collazo A, Keddam M, Novoa X, Takenouti H (1999) Cement paste hardening process studied by impedance spectroscopy. Electrochim Acta 44:4313–4318. https://doi.org/10.1016/S0013-4686(99)00147-4
20. Cui L, Cahyadi JH (2001) Permeability and pore structure of OPC paste. Cement Concr Res 31:277–282. https://doi.org/10.1016/S0008-8846(00)00474-9
21. Zhang J, Li Z (2009) Application of GEM equation in microstructure characterization of cement-based materials. J Mater Civil Eng 21:648–656. https://doi.org/10.1061/(ASCE)0899-1561(2009)21:11(648)
22. Neithalath N, Persun J, Manchiryal RK (2010) Electrical conductivity based microstructure and strength prediction of plain and modified concretes. Int J Adv Eng Sci Appl Math 2:83–94. https://doi.org/10.1007/s12572-011-0023-1
23. Snyder KA, Feng X, Keen BD, Mason TO (2003) Estimating the electrical conductivity of cement paste pore solutions from OH−, K+ and Na+ concentrations. Cement Concr Res 33:793–798. https://doi.org/10.1016/S0008-8846(02)01068-2
24. Kim H, Kim S, Yoon S (1995) Electrical properties of cement paste obtained from impedance spectroscopy. J Materials Sci 30:3768–3772. https://doi.org/10.1007/BF01153933
25. McLachlan DS, Blaszkiewicz M, Newnham RE (1990) Electrical resistivity of composites. J Am Ceram Soc

73:2187–2203. https://doi.org/10.1111/j.1151-2916.1990.tb07576.x
26. Li X, Caes S, Pardoen T, De Schutter G, Hauffman T, Kursten B (2023) Inhibition effect of lithium salts on the corrosion of AA1100 aluminium alloy in ordinary Portland cement pastes. Corros Sci 221:111325. https://doi.org/10.1016/j.corsci.2023.111325
27. Oh BH, Jang SY (2004) Prediction of diffusivity of concrete based on simple analytic equations. Cement Concr Res 34:463–480. https://doi.org/10.1016/j.cemconres.2003.08.026
28. Garboczi E, Bentz D (1992) Computer simulation of the diffusivity of cement-based materials. J Mater Sci 27:2083–2092. https://doi.org/10.1007/BF01117921
29. Garboczi EJ, Bentz DP (2001) The effect of statistical fluctuation, finite size error, and digital resolution on the phase percolation and transport properties of the NIST cement hydration model. Cement Concr Res 31:1501–1514. https://doi.org/10.1016/S0008-8846(01)00593-2
30. Prabhu A, Gimel JC, Ayuela A, Arrese-Igor S, Gaitero JJ, Dolado JS (2018) A multi-scale approach for percolation transition and its application to cement setting. Scientific Rep-UK 8:1–11. https://doi.org/10.1038/s41598-018-33918-6
31. Navi P, Pignat C (1996) Simulation of cement hydration and the connectivity of the capillary pore space. Adv Cem Based Mater 4:58–67. https://doi.org/10.1016/S1065-7355(96)90052-8
32. Tumidajski P, Schumacher A, Perron S, Gu P, Beaudoin J (1996) On the relationship between porosity and electrical resistivity in cementitious systems. Cement Concr Res 26:539–544. https://doi.org/10.1016/0008-8846(96)00017-8
33. Stauffer D, Aharony A (2003) Introduction to percolation theory. Taylor and Francis, England
34. Isichenko MB (1992) Percolation, statistical topography, and transport in random media. Rev Mod Phys 64:961. https://doi.org/10.1103/RevModPhys.64.961
35. Buenfeld N, Newman J (1987) Examination of three methods for studying ion diffusion in cement pastes, mortars and concrete. Mater Struct 20:3–10
36. Ma H, Hou D, Liu J, Li Z (2014) Estimate the relative electrical conductivity of C-S–H gel from experimental results. Constr Build Mater 71:392–396. https://doi.org/10.1016/j.conbuildmat.2014.08.036
37. Christensen BJ, Coverdale T, Olson RA, Ford SJ, Garboczi EJ, Jennings HM, Mason TO (1994) Impedance spectroscopy of hydrating cement-based materials: measurement, interpretation, and application. J Am Ceram Soc 77:2789–2804. https://doi.org/10.1111/j.1151-2916.1994.tb04507.x
38. Lizarazo-Marriaga J, Ramírez S, Fonseca L (2016) Influence of the aggregate–cement ratio on the electrical and transport properties of cement mortars. Arab J Sci Eng 41:4901–4909. https://doi.org/10.1007/s13369-016-2213-4
39. Krishna V, Kumar R (2016) Water to cement ratio: a simple and effective approach to control plastic and drying shrinkage in concrete. In: fourth international conference on sustainable construction materials and technology-proceeding. https://doi.org/10.18552/2016/SCMT4D139
40. Jennings HM, Kumar A, Sant G (2015) Quantitative discrimination of the nano-pore-structure of cement paste during drying: new insights from water sorption isotherms. Cement Concr Res 76:27–36. https://doi.org/10.1016/j.cemconres.2015.05.006
41. Bérubé M, Tremblay C, Fournier B, Thomas M, Stokes D (2004) Influence of lithium-based products proposed for counteracting ASR on the chemistry of pore solution and cement hydrates. Cement Concr Res 34:1645–1660. https://doi.org/10.1016/j.cemconres.2004.03.025
42. Olsson N, Baroghel-Bouny V, Nilsson LO, Thiery M (2013) Non-saturated ion diffusion in concrete – A new approach to evaluate conductivity measurements. Cement Concr Comp 40:40–47. https://doi.org/10.1016/j.cemconcomp.2013.04.001
43. Jain J, Neithalath N (2009) Analysis of calcium leaching behavior of plain and modified cement pastes in pure water. Cement Concr Comp 31:176–185. https://doi.org/10.1016/j.cemconcomp.2009.01.003
44. Diamond S (1999) Unique response of $LiNO_3$ as an alkali silica reaction-preventive admixture. Cement Concr Res 29:1271–1275. https://doi.org/10.1016/S0008-8846(99)00115-5
45. L'Hôpital E, Lothenbach B, Le Saout G, Kulik D, Scrivener K (2015) Incorporation of aluminium in calcium-silicate-hydrates. Cement Concr Res 75:91–103. https://doi.org/10.1016/j.cemconres.2015.04.007
46. Boel V, De Schutter G (2007) Determination of the porosity and the critical pore size of hardened self-compacting cement paste. In: 5th International RILEM Symposium on Self-Compacting Concrete (SCC 2007), pp 571–576.